Fluorine-terminated diamond (110) surfaces for nitrogen-vacancy quantum sensors

Wei Shen [a, c, d], Gai Wu [a, c, d], Lijie Li [b], Hui Li [a, c, d], Sheng Liu [a, c, d, *], Shengnan Shen [a, c, d, *], Diwei Zou [c, d]

[a] The Institute of Technological Sciences, Wuhan University, Wuhan 430074, China

[b] College of Engineering, Swansea University, Swansea, SA1 8EN, UK

[c] Research Institute of Wuhan University in Shenzhen, Shenzhen, 518057, China

[d] School of Power and Mechanical Engineering, Wuhan University, Wuhan, 430072, China

[*]Corresponding author.

E-mail: shengliu@whu.edu.cn (Sheng Liu)

E-mail: shen_shengnan@whu.edu.cn (Shengnan Shen)

Abstract: Diamond (110) surface is one of the low-index diamond faces but its effects on nitrogen-vacancy (NV) based quantum sensor remain unclear. The fluorine, hydrogen, nitrogen, and oxygen-terminated diamond (110) surfaces used for the NV centers are proposed here, and their electronic properties are investigated based on first-principles calculations. The oxygen-terminated diamond (110) surface has inter-bandgap states and surface electron spins, the nitrogen-terminated (110) surface has inter-band gap states, and the hydrogen-terminated (110) surface has negative electron affinity. Thus, these three surfaces may not be suitable for shallow NV centers. The fluorine-terminated diamond (110) surface has positive electron affinity, no surface related inter bandgap states, and no surface electron spins, so it is a promising candidate for NV-based quantum sensors.

Keywords: nitrogen-vacancy, quantum sensor, diamond (110) surface, fluorine termination

1. Introduction

The negatively charged nitrogen-vacancy (NV) center in diamond has long coherence time of milliseconds at room temperature, and its spin state can be optically read out and manipulated [1] [2]. The excellent spin properties make NV center gain much attention in the platform of quantum applications such as quantum computing [3], quantum network communication [4], and quantum sensing [5–7]. For its applications in quantum sensing, signal detection depends on the dipole coupling with the external targeted spins which decay with distance r as $1/r^3$ [8]. This requires the NV center to be located close to the diamond surface (<5 nm) [9], enhancing the sensitivity of the quantum sensor. Besides, the shallow NV center can provide higher spatial resolution, down to a few nanometres [10]. Particularly, for applications in biological quantum sensors, nanodiamonds with embedded NV centers can be utilized for living cell imaging, and the NV centers are inevitably close to the surface [11,12]. However, diamond surfaces have effects on the spin properties and charge stability of the shallow NV centers [13,14]. It is reported that the surface noise can reduce the spin relaxation times of shallow NV centers with depth less than 5 nm [15]. Ofori-Okai et al. [16] investigated the spin properties of NV centers with depth down to ~1 nm by optically detected magnetic-resonance spectroscopy. The spectral broadening of

shallow NV centers was observed which is related to the surface magnetic noise. The surface noise may originate from terminated atoms, surface dangling bonds or sp^2 carbon (C) [17,18]. In addition, the shallow NV centers exhibit decreased fluorescence contrast for optically detected electron spin resonance, because the surface terminations can make the charge state of the NV centers unstable [14,19]. Therefore, the surface engineering is significant important for the shallow NV centers [13,20,21].The hydrogen (H) is one of the most common terminations on the diamond surfaces. The difference in electronegativity (2.1 vs. 2.5) between H and carbon (C) results in a dipole moment directed toward the surface [22]. Thus, the H-terminated diamond (100) and (111) surfaces have negative electron affinity (NEA), which can induce a hole accumulation layer at the surface and a large upward band bending [23]. This will convert the shallow NV center to the positive charge state, and subsequently, to a nonfluorescent state. When changing the H to the oxygen (O), fluorine (F) or nitrogen (N) with electronegativity higher than carbon, the dipole moment directed away from the diamond surface will be set up, and the diamond surfaces exhibit positive electron affinity (PEA). The experimental studies have showed that O-terminated [24–26] and F-terminated [27] diamond (100) surfaces can keep the negative charge state of shallow NV centers and increase the fluorescence intensity. However, for O-terminated nanodiamonds, blinking states (temporary intermittency in fluorescence) of NV centers was observed [28]. For F-terminated diamond (100) surfaces, nearly 30% of NV centers exhibit permanent bleaching during the exposure to the laser [29]. The density functional theory (DFT) calculations [30] shows that O and F terminations on the diamond surfaces have surface related states in the band gap, and the excited electron of the NV center may be trapped in these states, leading to the blinking or bleaching. In addition, surface magnetic noise, originating from the surface terminations (e.g., dangling bonds), may limit the coherence time of shallow NV centers [31]. In summary, the three criteria of diamond surfaces used for NV-based quantum sensors are: PEA, no surface related states in the band gap, and no spin noises. Many types of diamond surfaces, which meet the three criteria simultaneously, have been proposed theoretically based on DFT calculations. These theoretically proposed surfaces include N-terminated [32], monolayer cubic boron nitride terminated [33], and epoxy oxidized [34] diamond (111) surfaces. Kawai et al. [35] has found N-terminated diamond (001) surface formed by nitrogen radical beam exposure can improve the spin properties of NV centers, compared with oxidized diamond surface. However, the N-terminated diamond (111) surfaces formed by RF(N_2) plasma exposure

are found to have C-N/C=N and C≡N bonds on the surface, which is different from the theoretically perfect N-terminated diamond (111) surfaces only with C-N bonds on the surface [32], and its effects on the NV center need further investigations.

Shallow NV centers are created mainly via three methods [36]: (i) *in situ* nitrogen delta-doping in chemical vapor deposition (CVD) diamond, (ii) nitrogen ion implantation into CVD diamond, (iii) carbon irradiation of N-doped high-pressure high-temperature (HPHT) diamond. The most common surfaces used in above three methods are diamond (100) [24,27,37–40] and (111) [41–43] surfaces, and effects of various terminations of diamond (100) [30,44] and (111) [32,34] surfaces on the near-surface NV centers have been widely studied. A single NV center can also be embedded in a nanodiamond to achieve nanoscale quantum sensing [45]. In contrast, diamond (110) surface is the least studied surface among the low-index faces that are relevant for NV-based sensor applications. The (110) surface is one of the most important surfaces for natural rough diamonds [46], a dominant surface for HPHT and CVD diamonds [47], and prevalent in nanodiamonds [48]. However, there is little research about shallow NV centers implanting in the (110) surface, and the effects of the diamond (110) surfaces on the NV-based quantum sensors have not been investigated either. In this work, we investigate the structural and the electronic properties of various diamond (110) surfaces and their effects on the NV centers, based on density functional theory calculations. A deep understanding of electronic properties of the (110) surfaces is important for paving the way to fabricate high-quality near-surface NV centers in the (110) surfaces.

2. Method

All the calculations are carried out by the plane-wave based PWmat code [49,50], with the generalized gradient approximation of Perdew-Burke-Ernzerhof (PBE) [51] and Optimized Norm-Conserving Vanderbilt pseudopotentials [52]. The energy cutoff of the plane-wave is set to 70 Ryd (~952.40 eV), and the convergence tolerance for the residual force and energy on each

atom during structure relaxation were set to 0.01 eV/Å and 2.72 × 10^{-6} eV, respectively. The diamond lattice parameter is calculated to be 3.565 Å, in excellent agreement with experimental value of 3.567 Å [53].

Surfaces are modeled using slabs with 18 carbon layers, and the vacuum layer thickness is set to about 16 Å to ensure that the interactions between the layers are negligible. The two layers in the middle of the slab are fixed during the relaxation. For the 1 × 2 supercells calculations, the Brillouin zone is sampled by an 8 × 6 × 1 Monkhorst–Pack *k*-points grid [54] for energy minimisation steps and a 16 × 12 × 1 *k*-points grid for density of states (DOS) calculations. The structural optimization is conducted with PBE functional to save the computation cost, while all the other calculations, such as electron affinity, DOS and band structure calculations, are performed with the hybrid functional of Hyed-Scuseria-Ernzerhof (HSE06) [55], which is nearly free of the electron self-interaction error and produces accurate electronic energy levels. The parameters are chosen after careful test calculations, as shown in Figs. S3-S7.

The electron affinity of diamond surfaces is defined as follows [56]:

$$E_{ea} = E_v - E_{slab,CBM} = E_v - (V_{slab} + E_{bulk,CBM} - V_{bulk}) \quad (1)$$

where E_v, $E_{slab,CBM}$, and V_{slab} refer to the vacuum energy, the conduction band minimum (CBM), and the average electrostatic potential of the diamond surface, respectively; $E_{bulk,CBM}$ and V_{bulk} are the CBM and the average electrostatic potential of bulk diamond, respectively. The $E_{bulk,CBM}$ derives from the valence band maximum (VBM) of bulk diamond plus the experimental value of band gap.

The formation enthalpy of diamond surface is expressed as [57]:

$$H(P,T) = [E_{slab+ab} - n_C\mu_C - \sum_i n_i\mu_i(P,T)]/\sum_i n_i \quad (2)$$

where n_C is the number of carbon atoms in the diamond surface and μ_C is the energy of carbon atom derived from bulk diamond; n_i is the number of the terminated atoms; $\mu_i(P,T)$ represents the chemical potential of the *i*th terminated atom under the pressure *P* and temperature *T*, which can be obtained from [58]:

$$\mu_i(P,T) = \mu_i(P^\circ,0) + H^\circ(T) - H^\circ(0) - TS^\circ(T) + k_B T ln(P/P^\circ) \quad (3)$$

where $\mu_i(P^\circ,0)$ is the energy of the atom at the temperature of 0 K and the standard-state pressure P°; $H^\circ(T)$ and $H^\circ(0)$ are the enthalpy of the atom at the temperature T and 0 K, respectively. $S^\circ(T)$ is the entropy of the atom at the temperature T; k_B is the Boltzmann constant; The enthalpy and entropy of the atom can be obtained from the thermodynamic tables [59].

3. Results and discussion

The relaxed bare diamond (110) surface exhibits unconstructed (1×1) configuration (see Fig. S1), in consistent with previous theoretical [60] and experimental [61] studies, and its structural parameters are listed in Table S3. In this work, four common elements (F, H, O, and N) are chosen to be adsorbed on the diamond (110) surfaces and saturate all the dangling bonds. And then, the electronic properties of these four types of surfaces are investigated by DFT calculations.

3.1 Structures and electronic properties

Geometric structures for 1 × 2 supercells of four diamond (110) surfaces are illustrated in Fig. 1. Bond lengths of various diamond (110) surfaces with different termination atoms after structural optimization are shown in Figure S1. The electron affinity of four surfaces is computed using PBE and HSE06 functionals, as shown in Table S3. The electron affinity of H-terminated diamond (110) surfaces and F-terminated surfaces by using PBE functional are consistent with results of previous studies (Table S3) [62,63]. These studies [62,63] only focused on the structures and electronic properties of H-terminated and F-terminated (110) surfaces and did not investigate the properties associated with diamond quantum sensors. The element H is less electronegative so the dipole moments directed toward the surface are established, while elements F, N, and O are more electronegative than C atoms so the dipole moments directed away from the surface are established. Although the PBE and HSE06 functionals give different

values of electron affinity, both of the calculation results based on two functionals show that H-terminated diamond (110) surface has NEA, while the other three types of surfaces have PEA. Due to the NEA, H-terminated diamond (110) surface may not be suitable for NV-based quantum sensors, which is similar with the cases of H-terminated diamond (100) and (111) surfaces.

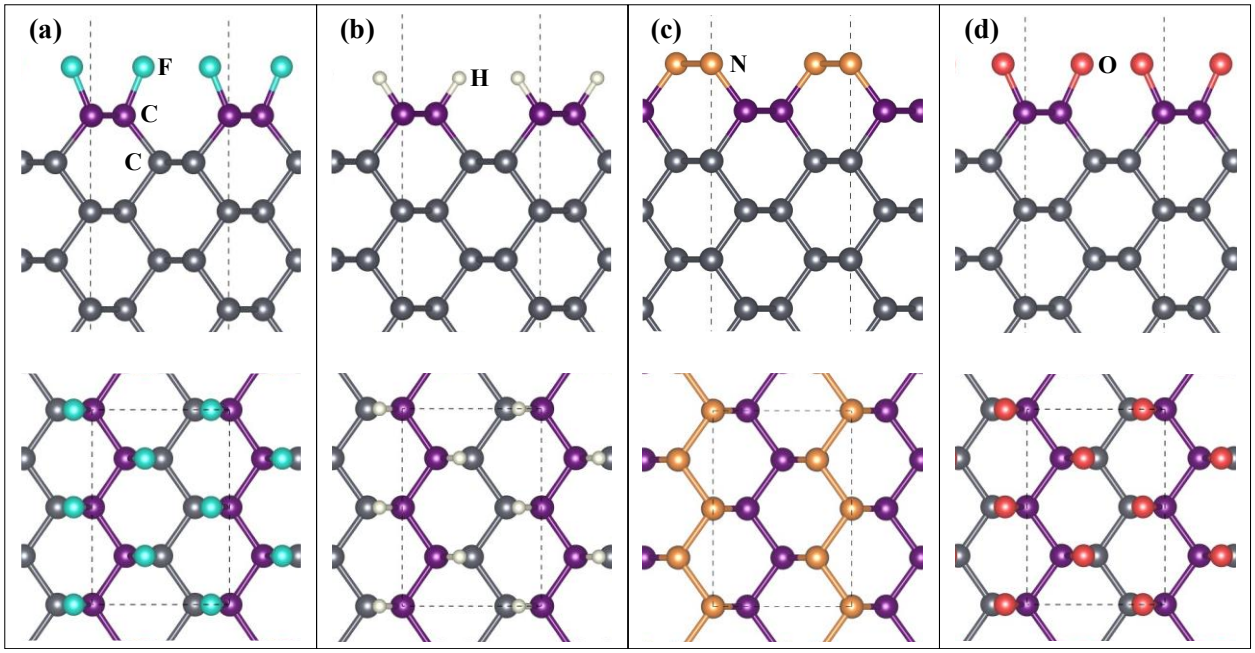

Figure 1. Side and top views of crystal structures: (a) F-terminated, (b) H-terminated, (c) N-terminated, and (d) O-terminated diamond (110) surfaces. Black dashed line denotes the structural 1 × 2 supercells. The F, H, N and O atoms are shown as green, white, orange and red circles, respectively. The C atoms in the top carbon layer and C atoms below the first carbon layer are shown as purple and grey atoms, respectively.

The calculations of partial density of states (PDOS) and fat band structure are performed using HSE06 functional, as shown in Fig. 2 and Fig. 3. To probe the origins of surface-related inter-bandgap states and the surface spins, the band decomposed charge density of the surface-related bands and spin density are computed, respectively, as show in Fig. 3. Calculations based on HSE06 functional is nearly free of the electron self-interaction error, so that HSE06 functional gives more accurate electronic levels in band gap than PBE functional [64]. Bulk C

atoms are chosen from the middle of the slab and their PDOS spectra indicate the position of the bandgap of bulk diamond. Surface C atoms are the atoms in the top carbon layer.

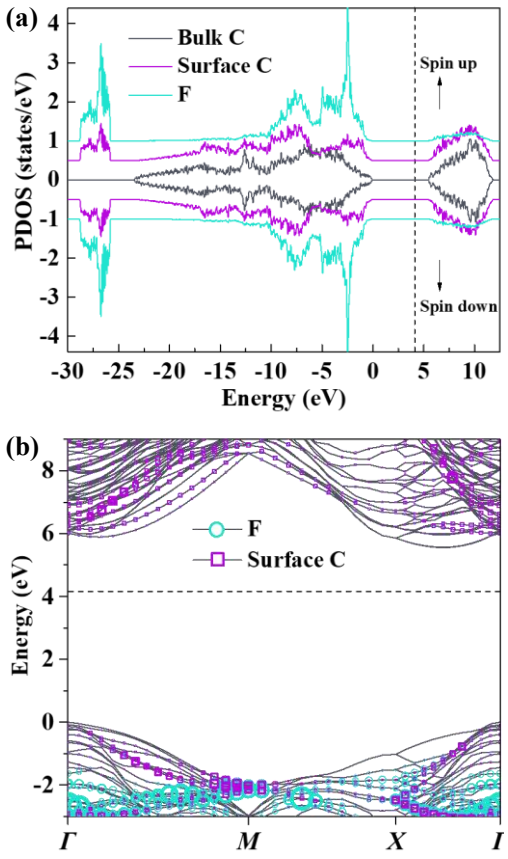

Figure 2. Electronic structures of the F-terminated diamond (110) surface. (a) PDOS spectra and (b) Band structure. The Fermi level is denoted by dashed lines. The bulk valence band maximum is set as energy zero.

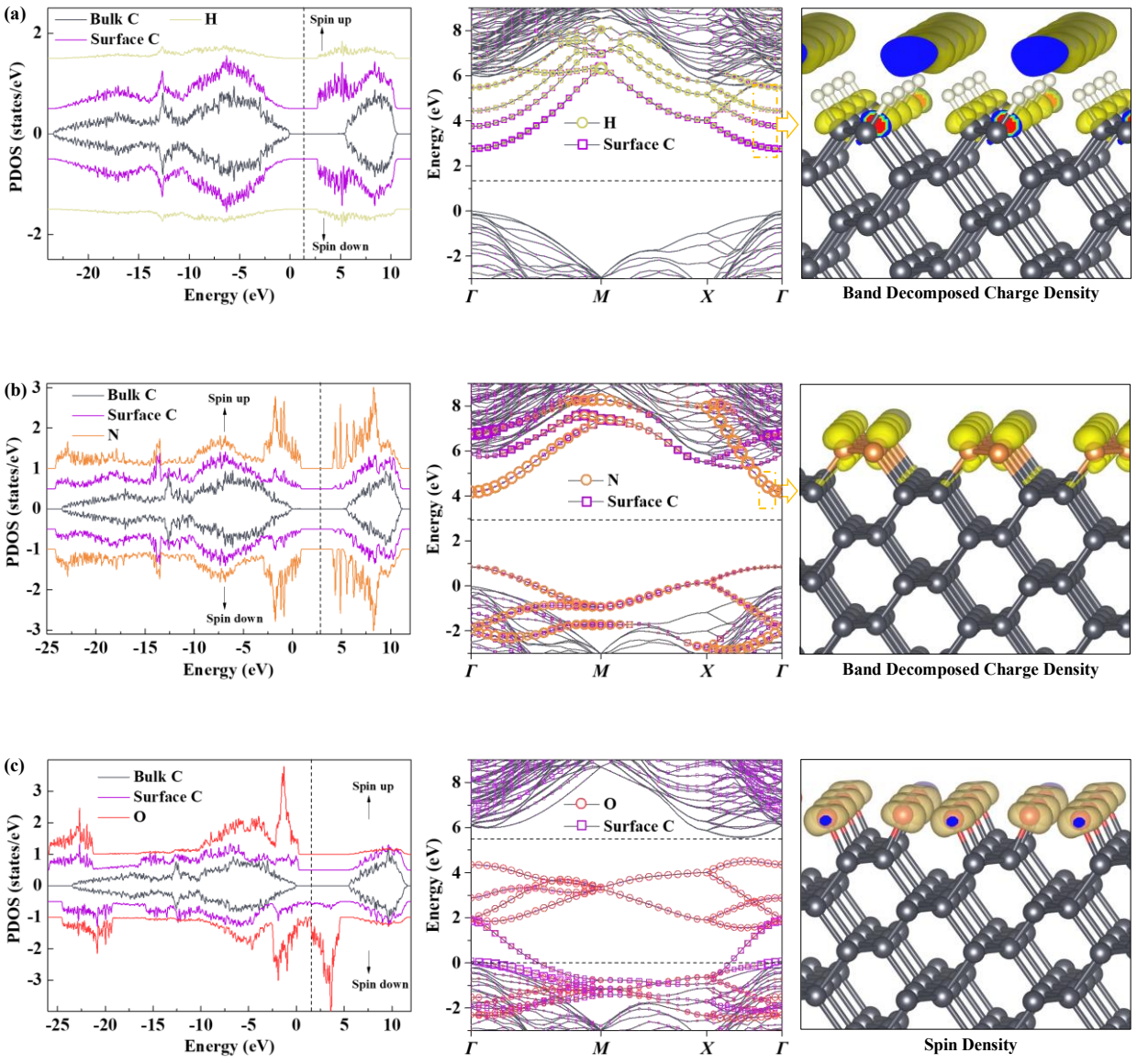

Figure 3. PDOS spectra, band structure, and charge density isosurface of (a) H-terminated, (b) N-terminated and (c) O-terminated diamond (110) surfaces. Charge density isosurface are depicted at isovalues of 0.17, 0.4, and 0.05 *e*/Bohr^3, respectively. The corresponding surface-related bands of band decomposed charge density are denoted by yellow dashed rectangle in band structures. The Fermi level is denoted by black dashed lines. The bulk valence band maximum is set as energy zero.

For F-terminated (110) surface, there is no inter-bandgap states and surface magnetic spin, as displayed in Fig. 2. The value of bandgap is calculated to be 5.53 eV, in consistent with its experimental value (5.47 eV) of bulk diamond. Thus, F-terminated diamond (110) surface meet

three criteria for applications of NV-based quantum sensors theoretically.

For H-terminated diamond (110) surface, there are many unoccupied states near the CBM, which may be mixed with the unoccupied levels of the NV center. Then the excited electron of the NV center could be trapped in these unoccupied states, leading to blinking or bleaching. The band decomposed charge density in Fig. 3 (a) shows that these unoccupied bands are the delocalized surface image states, which are called Rydberg states [65] in quantum chemistry. In the concept of Rydberg states, the lowest unoccupied states originate from the antibonding combination of the covalent bonds [33]. The strong sp^3 bonds in diamond produce the high level of antibonding combination, resulting a wide bandgap. The C−H covalent bond on the (110) surface is weaker than the sp^3 bond in the diamond, leading to low energy unoccupied levels under the CBM.

For N-terminated diamond (110) surface, there are also many unoccupied sub-band gap states. As presented in Fig. 3 (b), these sub-band states are *sp**-shape orbitals.

As displayed in Fig. 3 (c), O-terminated diamond (110) surface has inter-bandgap states and surface spins. The magnetic moments are localized around the O atoms, originating from the unpaired electron of the O atoms. It is similar with the case of on-top oxidized diamond (111) surfaces [34] which also have magnetic moments around the adsorbed O atoms.

Therefore, H-, N-, and O-terminated diamond (110) surfaces may not be suitable for NV-based quantum sensors theoretically.

3.2 Surface stability

Ab initio molecular dynamics (AIMD) simulations with the PBE functional is conducted to examine the stability of F-terminated diamond (110) surfaces. The structure in AIMD simulations is a 3 × 5 supercell composed of seven carbon layers. The lowest-lying carbon layers with their terminating H atoms are frozen to simulate the constraint induced by the bulk. As displayed in the Fig. 4, AIMD simulation shows that the F-terminated surface structure are robust after 10 ps at 500 K, suggesting thermal stabilities at ambient conditions.

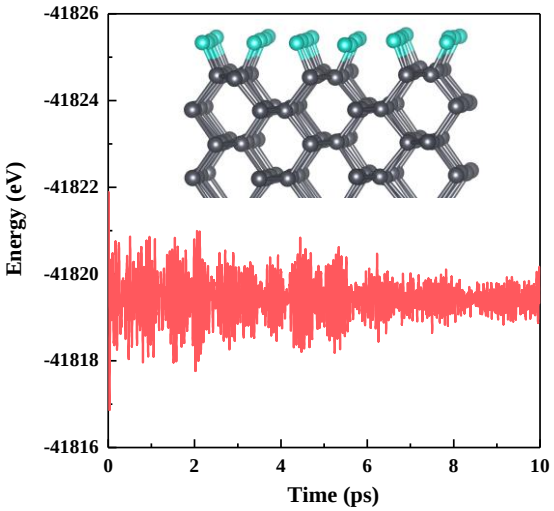

Figure 4. Evolution of the total energy of the F-terminated diamond (110) surface with a temperature of 500 K. The inset is AIMD snapshots of the surface at the time of 10 ps.

The pressure and temperature-dependent formation enthalpies are calculated to confirm the surface stability and investigate the possibility of fabricating F-terminated diamond (110) surface by chemical vapor deposition. As shown in Fig. 5, the formation enthalpy decreases with the increase of the pressure or with the decrease of the temperature. For example, the surface is stable under ~785 K in the pressure of 2×10^{-5} Torr or under ~1100 K in the pressure of 2 Torr. Compared with pressure, temperature has a stronger influence on the stability of the F-terminated (110) surface. Therefore, fabrication of F-terminated diamond (110) surface should be under a relatively low temperature (< ~700K). Fluorination on the diamond (100) surface has been achieved by exposing surfaces to fluorine-containing gases (e.g., F [66], XeF_2 [67]) and plasmas (e.g., CF_4 [68], CF [69]). Previous annealing experiments show that terminated F atoms start to desorb from the diamond (100) surface above the temperature of ~925 °C [67]. Similarly, the F-terminated diamond (100) surface is stable under a relatively low temperature.

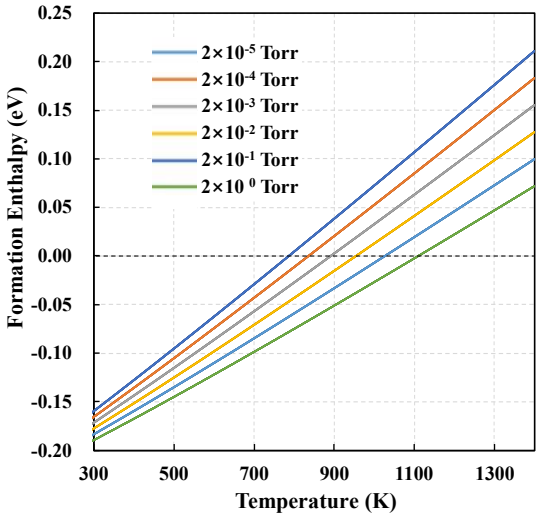

Figure 5. Pressure and temperature-dependent formation enthalpies of F-terminated diamond (110) surfaces

3.3 Effects on the NV center

In order to outline the effect of the F terminations on the NV center, calculations on a 3 × 5 supercell with a single NV center are also performed. An NV center is placed in the middle of the supercell and a substitutional N atom is also placed at the same layer with a distance of 7.67 Å from the NV center, as shown in Fig. 6 (a). The distance is larger than 7.5 Å, which ensures that the substitutional N has a minimal effect on the NV center [70]. The depth of the NV center is ~11.5 Å. The local structural parameters of NV center and substitutional N are shown in Fig. S2 and Table S2. For (001) [71] and (111) [34] surfaces, the depth deeper than 10 Å means the NV centers properties have already converged to bulk values. Firstly, a 3 × 5 supercell of F-termination surface without NV center or additional N atom is built and relaxed. Then the NV center and additional N atom are introduced in the supercell, and the terminated atom and the first carbon layer are fixed during the relaxation. The gamma point and PBE functional are used during the geometry optimization. The energy cutoff of the plane-wave is reduced to 50 Ryd to save the computational costs. The substitutional N atom acts as the electron donor to NV center and makes the NV center in the negative charge state, to achieve an uncharged supercell.

Conventional way to charge the NV center is making the supercell in negative charge state without the donor N, and then an artificial background jellium charge is imposed. However, in the case of charged defects, the Coulomb interaction between the localized charge distributions converges very slowly and many approaches have been proposed over the years to overcome this problem [72,73]. By contrast, the method of introducing donor N can avoid solving this problem.

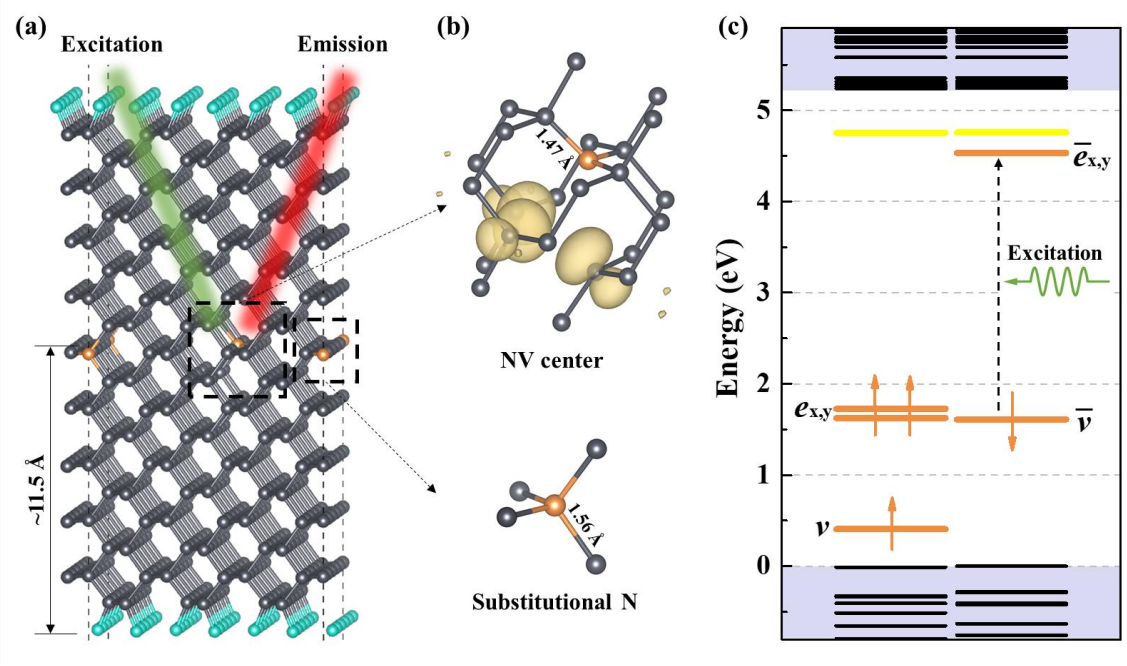

Figure 6. (a) Structure of 3×5 supercell of F-terminated diamond (110) surface. The NV center is excited by green light to emit in the red range. (b) Spin density of NV center calculated by HSE06 functional and the substitutional N. Charge density isosurface is depicted at isovalue of 0.011 e/Bohr^3. (c) Defect levels of NV center in the supercell calculated by HSE06 functional. The orange and yellow lines represent the levels of NV center and substitutional N, respectively.

The HSE06 computed spin density for ground state of NV center is shown in Fig. 6 (b), while the substitutional N has zero spin density. As shown in Fig. 6 (c), there are no extra surface-related levels in the band gap, which is identical to the band structure in Fig. 2. The splitting of the occupied level $e_{x,y}$ is nearly 0.1 eV, but the splitting of the unoccupied $\bar{e}_{x,y}$ level is small as about 1.8 meV. The luminescence of NV center is from the $\bar{e}_{x,y}$-to-$\bar{v}_{x,y}$

electronic transition, and splitting of these two levels can bring luminescence broadening, and then reduce the luminescence intensity [44]. Thus, for the NV center in F-terminated (110) surface, splitting of the occupied level $e_{x,y}$ may not affect the luminescence, and the small splitting value of the unoccupied $\bar{e}_{x,y}$ level will not lead to obvious luminescence broadening. Energy diagram illustrating the Franck–Condon approximation for the excitation and de-excitation process of the NV center is shown in Fig. S8. The optical transitions of the NV center in F-terminated (110) surface are calculated by PBE and HSE06 functional are presented in Table S4, which agrees well with previous studies [64]. For example, the HSE06 calculated zero-phonon-line of the NV center is 1.910 eV, close to the theoretical value (1.955 eV [64], 1.962 eV [70]) and experimental value (1.945 eV [74]) of NV center in bulk diamond. Therefore, it is confirmed that F terminations on the (110) surface have no obvious effects on the optical properties of the shallow NV center (depth ≈ 11.5 Å). Furthermore, the effects of the depth of NV center on the optical properties are shown in Figs. S9-12.

In this work, F termination is proved to be more suitable for shallow NV centers than O termination on diamond (110) surface based on DFT calculations. Actually, the most widely used termination on the diamond (100) and (111) surfaces for quantum sensors is oxygen [24,27–29,75]. For example, Hayate et al. [76] found that surface oxidization can stabilize the charge state of shallow NV center and improve their coherence properties evaluated using Rabi oscillation measurements. Lovchinsky et al. [77] used the shallow NV centers to detect single proteins, and they found that the surface treatment is important for detection sensitivity. Their experiments show that the coherence time can be improved by more than an order of magnitude when the diamond surface is oxidized combined with annealing. The oxygen is bioinert material which is required in biological sensing [78,79], while fluorine is not bioinert material. In addition, oxygen does not have nuclear spins while fluorine has nuclear spins. The nuclear spins will produce nuclear spin noise in quantum sensing [80]. However, for F-terminated diamond (111) or (001) surfaces, the resulting surface dipole is directed away from the surface and is very strong because the electronegativity difference between F (4.0) and surface C (2.5) is very large [22]. Thus, the F-terminated diamond surface is highly water-repellent, avoiding the nonspecific binding of biomolecules [22]. This property is important, because one of the applications of NV

centers is biological sensing. Therefore, it is deduced that F-terminated diamond (110) surface can be chemically stable in bio-sensing applications. In addition, the charge states of NV centers are more stable on the F-terminated (100) surface than the O-terminated (100) surface [68]. This could be explained by that O-terminated (100) surface exist a mixed chemical state with hydroxyl groups or carboxylic acids and could reaction with moisture in air which is likely to become electron acceptors [68]. Therefore, for these reasons, fluorine terminations may perform better than oxygen terminations on the diamond (110) surface for biological quantum sensors.

We strive to provide a comprehensive list of studies related to the effects of surface terminations on the NV centers, as shown in Table S5. Many other significantly important studies of NV centers, which are not related to surface terminations, may not be listed in this work. Theoretically, F-terminated diamond (110) surface meets the three criteria: PEA, no surface related states in the band gap, and no spin noises. Therefore, F-terminated diamond (110) surface performs better over many other terminated diamond surfaces, as shown in the Table S5. In addition, this is the first work investigating the effects of (110) surface terminations on the NV centers, intending to invoke further research on the diamond (110) surfaces.

Then, we turn to discuss the differences among the (110) surface and other surface orientations used for NV centers. For the CVD-grown diamond, the alignment of NV centers is up to ~100% [41], 50% [81], 50% [81], and 73% [80] on (111), (100), (110), and (113) surfaces, respectively. Preferentially-aligned NV centers will increase the number of collected photons and then the signal-to-noise ratio in quantum sensing applications [42]. Thus, from the perspective of alignment of NV centers, CVD-grown (110) surfaces may not be the best surface compared with CVD-grown (111) surfaces. However, ion implantation and carbon irradiation are the other two common methods producing NV centers. For these two methods, NV centers are randomly oriented along four <111> crystallographic axes, and therefore in these two methods, there is no differences in alignment of NV centers among (111), (100), (110), and (113) surfaces.

4. Conclusions

To summarize, F, O, H, and N-terminated diamond (110) surfaces used for shallow NV centers

are first proposed in this work, and their electronic properties are investigated based on DFT calculations. The O-terminated diamond (110) surface has inter-bandgap states and surface electron spins, the N-terminated diamond (110) surface has inter-band gap states, and the H-terminated diamond (110) surface has NEA. Thus, these three surfaces may not be suitable for shallow NV centers. The F-terminated diamond (110) surface has PEA, no surface related inter bandgap states, and no surface electron spins, so it may be suitable for NV-based quantum sensors. Furthermore, an NV center is placed in the F-terminated diamond (110) surface and it is confirmed that F terminations have no obvious effects on the electronic and optical properties of NV center. The AIMD simulation shows that the F-terminated surface is thermally stable at 500 K. The formation enthalpy calculations results indicate that fabrication of F-terminated diamond (110) surface should be under a relatively low temperature (< ~700K). This work will pave the way to fabricate high-quality near-surface NV centers in the (110) surfaces.

Declaration of competing interest

The authors declare no conflict of interest.

Acknowledgements

This work is funded by the National Natural Science Foundation of China (51727901, 62004141), the Guandong Basic and Applied Basic Research Fund: Guangdong-Shenzhen Joint Fund (2020B1515120005), and the Science and Technology Facilities Council (ST/T006455/1).

Author contributions

Wei Shen and Gai Wu contributed equally to this work.

Appendix A. Supporting information

Supplementary Figures S1–S12 and Tables S1–S5.

References

[1] D.M. Irber, F. Poggiali, F. Kong, M. Kieschnick, T. Lühmann, D. Kwiatkowski, J. Meijer, J. Du, F. Shi, F. Reinhard, Robust all-optical single-shot readout of nitrogen-vacancy centers in diamond, Nat. Commun. 12 (2021) 1–6. https://doi.org/10.1038/s41467-020-20755-3.

[2] N. Savage, Quantum diamond sensors, Nature. 591 (2021) S37–S37. https://doi.org/10.1038/d41586-021-00742-4.

[3] J. Zhang, S.S. Hegde, D. Suter, Efficient implementation of a quantum algorithm in a single nitrogen-vacancy center of diamond, Phys. Rev. Lett. 125 (2020) 30501. https://doi.org/10.1103/PhysRevLett.125.030501.

[4] W. Pfaff, B.J. Hensen, H. Bernien, S.B. van Dam, M.S. Blok, T.H. Taminiau, M.J. Tiggelman, R.N. Schouten, M. Markham, D.J. Twitchen, Unconditional quantum teleportation between distant solid-state quantum bits, Science. 345 (2014) 532–535. https://doi.org/10.1126/science.1253512.

[5] J.J. Hamlin, B.B. Zhou, Extreme diamond-based quantum sensors, Science. 366 (2019) 1312–1313. https://doi.org/10.1126/science.aaz4982.

[6] V. V Soshenko, S. V Bolshedvorskii, O. Rubinas, V.N. Sorokin, A.N. Smolyaninov, V. V Vorobyov, A. V Akimov, Nuclear spin gyroscope based on the nitrogen vacancy center in diamond, Phys. Rev. Lett. 126 (2021) 197702. https://doi.org/10.1103/PhysRevLett.126.197702.

[7] Y. Xie, H. Yu, Y. Zhu, X. Qin, X. Rong, C.-K. Duan, J. Du, A hybrid magnetometer towards femtotesla sensitivity under ambient conditions, Sci. Bull. 66 (2021) 127–132. https://doi.org/10.1016/j.scib.2020.08.001.

[8] K. Ohno, F. Joseph Heremans, L.C. Bassett, B.A. Myers, D.M. Toyli, A.C. Bleszynski

Jayich, C.J. Palmstrøm, D.D. Awschalom, Engineering shallow spins in diamond with nitrogen delta-doping, Appl. Phys. Lett. 101 (2012) 82413. https://doi.org/10.1063/1.4748280.

[9] F. Fávaro de Oliveira, S.A. Momenzadeh, Y. Wang, M. Konuma, M. Markham, A.M. Edmonds, A. Denisenko, J. Wrachtrup, Effect of low-damage inductively coupled plasma on shallow nitrogen-vacancy centers in diamond, Appl. Phys. Lett. 107 (2015) 73107. https://doi.org/10.1063/1.4929356.

[10] J.-P. Tetienne, R.W. De Gille, D.A. Broadway, T. Teraji, S.E. Lillie, J.M. McCoey, N. Dontschuk, L.T. Hall, A. Stacey, D.A. Simpson, Spin properties of dense near-surface ensembles of nitrogen-vacancy centers in diamond, Phys. Rev. B. 97 (2018) 85402. https://doi.org/10.1103/PhysRevB.97.085402.

[11] S. Castelletto, L. Rosa, A. Boretti, Micro-manipulation of nanodiamonds containing NV centers for quantum applications, Diam. Relat. Mater. 106 (2020) 107840. https://doi.org/10.1016/j.diamond.2020.107840.

[12] H.C. Davis, P. Ramesh, A. Bhatnagar, A. Lee-Gosselin, J.F. Barry, D.R. Glenn, R.L. Walsworth, M.G. Shapiro, Mapping the microscale origins of magnetic resonance image contrast with subcellular diamond magnetometry, Nat. Commun. 9 (2018) 131. https://doi.org/10.1038/s41467-017-02471-7.

[13] Á. Gali, Ab initio theory of the nitrogen-vacancy center in diamond, Nanophotonics. 8 (2019) 1907–1943. https://doi.org/10.1515/nanoph-2019-0154.

[14] D. Bluvstein, Z. Zhang, A.C.B. Jayich, Identifying and mitigating charge instabilities in shallow diamond nitrogen-vacancy centers, Phys. Rev. Lett. 122 (2019) 76101. https://doi.org/10.1103/PhysRevLett.122.076101.

[15] T. Rosskopf, A. Dussaux, K. Ohashi, M. Loretz, R. Schirhagl, H. Watanabe, S. Shikata, K.M. Itoh, C.L. Degen, Investigation of Surface Magnetic Noise by Shallow Spins in Diamond, Phys. Rev. Lett. 112 (2014) 147602. https://doi.org/10.1103/PhysRevLett.112.147602.

[16] B.K. Ofori-Okai, S. Pezzagna, K. Chang, M. Loretz, R. Schirhagl, Y. Tao, B.A. Moores, K. Groot-Berning, J. Meijer, C.L. Degen, Spin properties of very shallow nitrogen vacancy defects in diamond, Phys. Rev. B. 86 (2012) 81406. https://doi.org/10.1103/PhysRevB.86.081406.

[17] A. Stacey, N. Dontschuk, J.-P. Chou, D.A. Broadway, A.K. Schenk, M.J. Sear, J.-P. Tetienne, A. Hoffman, S. Prawer, C.I. Pakes, A. Tadich, N.P. de Leon, A. Gali, L.C.L. Hollenberg, Evidence for primal sp2 defects at the diamond surface: candidates for electron trapping and noise sources, Adv. Mater. Interfaces. 6 (2019) 1801449. https://doi.org/10.1002/admi.201801449.

[18] S.E. Lillie, D.A. Broadway, N. Dontschuk, A. Zavabeti, D.A. Simpson, T. Teraji, T. Daeneke, L.C.L. Hollenberg, J.-P. Tetienne, Magnetic noise from ultrathin abrasively deposited materials on diamond, Phys. Rev. Mater. 2 (2018) 116002. https://doi.org/10.1103/PhysRevMaterials.2.116002.

[19] Z. Yuan, M. Fitzpatrick, L.V.H. Rodgers, S. Sangtawesin, S. Srinivasan, N.P. de Leon, Charge state dynamics and optically detected electron spin resonance contrast of shallow nitrogen-vacancy centers in diamond, Phys. Rev. Res. 2 (2020) 33263. https://doi.org/10.1103/PhysRevResearch.2.033263.

[20] S. Dhomkar, H. Jayakumar, P.R. Zangara, C.A. Meriles, Charge Dynamics in near-Surface, Variable-Density Ensembles of Nitrogen-Vacancy Centers in Diamond, Nano Lett. 18 (2018) 4046–4052. https://doi.org/10.1021/acs.nanolett.8b01739.

[21] K. Liu, S. Zhang, V. Ralchenko, P. Qiao, J. Zhao, G. Shu, L. Yang, J. Han, B. Dai, J. Zhu, Tailoring of Typical Color Centers in Diamond for Photonics, Adv. Mater. 33 (2021) 2000891. https://doi.org/10.1002/adma.202000891.

[22] H. Kawarada, A.R. Ruslinda, Diamond electrolyte solution gate FETs for DNA and protein sensors using DNA/RNA aptamers, Phys. Status Solidi. 208 (2011) 2005–2016. https://doi.org/10.1002/pssa.201100503.

[23] J.-P. Chou, A. Gali, Nitrogen-vacancy diamond sensor: novel diamond surfaces from ab

initio simulations, MRS Commun. 7 (2017) 551–562. https://doi.org/10.1557/mrc.2017.75.

[24] M. V Hauf, B. Grotz, B. Naydenov, M. Dankerl, S. Pezzagna, J. Meijer, F. Jelezko, J. Wrachtrup, M. Stutzmann, F. Reinhard, Chemical control of the charge state of nitrogen-vacancy centers in diamond, Phys. Rev. B. 83 (2011) 81304. https://doi.org/10.1103/PhysRevB.83.081304.

[25] M. Kim, H.J. Mamin, M.H. Sherwood, C.T. Rettner, J. Frommer, D. Rugar, Effect of oxygen plasma and thermal oxidation on shallow nitrogen-vacancy centers in diamond, Appl. Phys. Lett. 105 (2014). https://doi.org/10.1063/1.4891839.

[26] G. Braunbeck, S. Mandal, M. Touge, O.A. Williams, F. Reinhard, Effect of ultraprecision polishing techniques on coherence times of shallow nitrogen-vacancy centers in diamond, Diam. Relat. Mater. 85 (2018) 18–22. https://doi.org/10.1016/j.diamond.2018.03.026.

[27] C. Osterkamp, J. Scharpf, S. Pezzagna, J. Meijer, T. Diemant, R. Jürgen Behm, B. Naydenov, F. Jelezko, Increasing the creation yield of shallow single defects in diamond by surface plasma treatment, Appl. Phys. Lett. 103 (2013) 193118.

[28] C. Bradac, T. Gaebel, C.I. Pakes, J.M. Say, A. V Zvyagin, J.R. Rabeau, Effect of the nanodiamond host on a nitrogen-vacancy color-centre emission state, Small. 9 (2013) 132–139. https://doi.org/10.1002/smll.201200574.

[29] K. Ohashi, T. Rosskopf, H. Watanabe, M. Loretz, Y. Tao, R. Hauert, S. Tomizawa, T. Ishikawa, J. Ishi-Hayase, S. Shikata, C.L. Degen, K.M. Itoh, Negatively charged nitrogen-vacancy centers in a 5 nm thin 12C diamond film, Nano Lett. 13 (2013) 4733–4738. https://doi.org/10.1021/nl402286v.

[30] M. Kaviani, P. Deák, B. Aradi, T. Frauenheim, J.-P. Chou, A. Gali, Proper surface termination for luminescent near-surface NV centers in diamond, Nano Lett. 14 (2014) 4772–4777. https://doi.org/10.1021/nl501927y.

[31] Y. Romach, C. Müller, T. Unden, L.J. Rogers, T. Isoda, K.M. Itoh, M. Markham, A. Stacey, J. Meijer, S. Pezzagna, B. Naydenov, L.P. McGuinness, N. Bar-Gill, F. Jelezko,

Spectroscopy of surface-induced noise using shallow spins in diamond, Phys. Rev. Lett. 114 (2015) 1–5. https://doi.org/10.1103/PhysRevLett.114.017601.

[32] J.-P. Chou, A. Retzker, A. Gali, Nitrogen-terminated diamond (111) surface for room-temperature quantum sensing and simulation, Nano Lett. 17 (2017) 2294–2298. https://doi.org/10.1021/acs.nanolett.6b05023.

[33] W. Shen, S. Shen, S. Liu, H. Li, Z. Gan, Q. Zhang, Monolayer cubic boron nitride terminated diamond (111) surfaces for quantum sensing and electron emission applications, ACS Appl. Mater. Interfaces. 12 (2020) 33336–33345. https://doi.org/10.1021/acsami.0c05268.

[34] W. Shen, S. Shen, S. Liu, H. Li, Y. Zhang, Q. Zhang, Y. Guo, Epoxy oxidized diamond (111)-(2× 1) surface for nitrogen-vacancy based quantum sensors, Carbon N. Y. 173 (2021) 485–492. https://doi.org/10.1016/j.carbon.2020.11.037.

[35] S. Kawai, H. Yamano, T. Sonoda, K. Kato, J.J. Buendia, T. Kageura, R. Fukuda, T. Okada, T. Tanii, T. Higuchi, M. Haruyama, K. Yamada, S. Onoda, T. Ohshima, W. Kada, O. Hanaizumi, A. Stacey, T. Teraji, S. Kono, J. Isoya, H. Kawarada, Nitrogen-Terminated Diamond Surface for Nanoscale NMR by Shallow Nitrogen-Vacancy Centers, J. Phys. Chem. C. 123 (2019) 3594–3604. https://doi.org/10.1021/acs.jpcc.8b11274.

[36] A.J. Healey, A. Stacey, B.C. Johnson, D.A. Broadway, T. Teraji, D.A. Simpson, J.-P. Tetienne, L.C.L. Hollenberg, Comparison of different methods of nitrogen-vacancy layer formation in diamond for wide-field quantum microscopy, Phys. Rev. Mater. 4 (2020) 104605. https://doi.org/10.1103/PhysRevMaterials.4.104605.

[37] T. Jaffe, M. Attrash, M.K. Kuntumalla, R. Akhvlediani, S. Michaelson, L. Gal, N. Felgen, M. Fischer, J.P. Reithmaier, C. Popov, Novel ultra localized and dense nitrogen delta-doping in diamond for advanced quantum sensing, Nano Lett. 20 (2020) 3192–3198. https://doi.org/10.1021/acs.nanolett.9b05243.

[38] W. Zhang, J. Zhang, J. Wang, F. Feng, S. Lin, L. Lou, W. Zhu, G. Wang, Depth-dependent decoherence caused by surface and external spins for NV centers in

diamond, Phys. Rev. B. 96 (2017) 235443. https://doi.org/10.1103/PhysRevB.96.235443.

[39] G. Wu, M.-H. Chen, J. Liao, The influence of recess depth and crystallographic orientation of seed sides on homoepitaxial growth of CVD single crystal diamonds, Diam. Relat. Mater. 65 (2016) 144–151. https://doi.org/10.1016/j.diamond.2016.03.011.

[40] G. Wu, Q. Wang, Y. Wu, X. Sun, J. Liao, J. Pan, M. Chen, M. Kasu, S. Liu, Evolution of defects, morphologies and fundamental growth characteristics of CVD diamond films induced by nitrogen addition, Mater. Today Commun. 25 (2020) 101504. https://doi.org/10.1016/j.mtcomm.2020.101504.

[41] H. Ozawa, K. Tahara, H. Ishiwata, M. Hatano, T. Iwasaki, Formation of perfectly aligned nitrogen-vacancy-center ensembles in chemical-vapor-deposition-grown diamond (111), Appl. Phys. Express. 10 (2017) 45501. https://doi.org/10.7567/apex.10.045501.

[42] H. Ozawa, Y. Hatano, T. Iwasaki, Y. Harada, M. Hatano, Formation of perfectly aligned high-density NV centers in (111) CVD-grown diamonds for magnetic field imaging of magnetic particles, Jpn. J. Appl. Phys. 58 (2019) SIIB26. https://doi.org/10.7567/1347-4065/ab203c.

[43] J. Michl, T. Teraji, S. Zaiser, I. Jakobi, G. Waldherr, F. Dolde, P. Neumann, M.W. Doherty, N.B. Manson, J. Isoya, Perfect alignment and preferential orientation of nitrogen-vacancy centers during chemical vapor deposition diamond growth on (111) surfaces, Appl. Phys. Lett. 104 (2014) 102407. https://doi.org/10.1063/1.4868128.

[44] H. Pinto, R. Jones, D.W. Palmer, J.P. Goss, A.K. Tiwari, P.R. Briddon, N.G. Wright, A.B. Horsfall, M.J. Rayson, S. Öberg, First-principles studies of the effect of (001) surface terminations on the electronic properties of the negatively charged nitrogen-vacancy defect in diamond, Phys. Rev. B. 86 (2012) 45313. https://doi.org/10.1103/PhysRevB.86.045313.

[45] K. Fukushige, H. Kawaguchi, K. Shimazaki, T. Tashima, H. Takashima, S. Takeuchi, Identification of the orientation of a single NV center in a nanodiamond using a three-dimensionally controlled magnetic field, Appl. Phys. Lett. 116 (2020) 264002.

https://doi.org/10.1063/5.0009698.

[46] G. Francz, P. Kania, G. Gantner, H. Stupp, P. Oelhafen, Photoelectron spectroscopy study of natural (100),(110),(111) and CVD diamond surfaces, Phys. Status Solidi. 154 (1996) 91–108. https://doi.org/10.1002/pssa.2211540109.

[47] R.S. Balmer, J.R. Brandon, S.L. Clewes, H.K. Dhillon, J.M. Dodson, I. Friel, P.N. Inglis, T.D. Madgwick, M.L. Markham, T.P. Mollart, N. Perkins, G.A. Scarsbrook, D.J. Twitchen, A.J. Whitehead, J.J. Wilman, S.M. Woollard, Chemical vapour deposition synthetic diamond: materials, technology and applications, J. Phys. Condens. Matter. 21 (2009) 364221. https://doi.org/10.1088/0953-8984/21/36/364221.

[48] L. Lai, A.S. Barnard, Stability of nanodiamond surfaces exposed to N, NH, and NH2, J. Phys. Chem. C. 115 (2011) 6218–6228. https://doi.org/10.1021/jp1111026.

[49] W. Jia, Z. Cao, L. Wang, J. Fu, X. Chi, W. Gao, L.-W. Wang, The analysis of a plane wave pseudopotential density functional theory code on a GPU machine, Comput. Phys. Commun. 184 (2013) 9–18. https://doi.org/10.1016/j.cpc.2012.08.002.

[50] W. Jia, J. Fu, Z. Cao, L. Wang, X. Chi, W. Gao, L.-W. Wang, Fast plane wave density functional theory molecular dynamics calculations on multi-GPU machines, J. Comput. Phys. 251 (2013) 102–115. https://doi.org/10.1016/j.jcp.2013.05.005.

[51] J.P. Perdew, K. Burke, M. Ernzerhof, Generalized gradient approximation made simple, Phys. Rev. Lett. 77 (1996) 3865–3868. https://doi.org/10.1103/PhysRevLett.77.3865.

[52] D.R. Hamann, Optimized norm-conserving Vanderbilt pseudopotentials, Phys. Rev. B. 88 (2013) 85117. https://doi.org/10.1103/PhysRevB.88.085117.

[53] T. Hom, W. Kiszenik, B. Post, Accurate lattice constants from multiple reflection measurements. II. Lattice constants of germanium silicon, and diamond, J. Appl. Crystallogr. 8 (1975) 457–458. https://doi.org/10.1107/S0021889875010965.

[54] H.J. Monkhorst, J.D. Pack, Special points for Brillouin-zone integrations, Phys. Rev. B. 13 (1976) 5188–5192. https://doi.org/10.1103/PhysRevB.13.5188.

[55] A. V. Krukau, O.A. Vydrov, A.F. Izmaylov, G.E. Scuseria, Influence of the exchange

screening parameter on the performance of screened hybrid functionals, J. Chem. Phys. 125 (2006) 224106. https://doi.org/10.1063/1.2404663.

[56] W. Shen, Y. Pan, S. Shen, H. Li, Y. Zhang, G. Zhang, Electron affinity of boron-terminated diamond (001) surfaces: a density functional theory study, J. Mater. Chem. C. 7 (2019) 9756–9765. https://doi.org/10.1039/C9TC02517K.

[57] K. Reuter, M. Scheffler, Composition, structure, and stability of RuO 2 (110) as a function of oxygen pressure, Phys. Rev. B. 65 (2001) 35406. https://doi.org/10.1103/PhysRevB.65.035406.

[58] A.P. Seitsonen, A.M. Saitta, T. Wassmann, M. Lazzeri, F. Mauri, Structure and stability of graphene nanoribbons in oxygen, carbon dioxide, water, and ammonia, Phys. Rev. B. 82 (2010) 115425. https://doi.org/10.1103/PhysRevB.82.115425.

[59] M.W.J. CHASE, NIST-JANAF Thermochemical Tables Fourth Edition, J. Phys. Chem. Ref. Data, Monogr. 9 (1998). https://ci.nii.ac.jp/naid/10026079537/en/.

[60] G. Kern, J. Hafner, Ab initio calculations of the atomic and electronic structure of diamond (111) surfaces with steps, Phys. Rev. B. 58 (1998) 2161–2169. https://doi.org/10.1103/PhysRevB.58.2161.

[61] F. Maier, R. Graupner, M. Hollering, L. Hammer, J. Ristein, L. Ley, The hydrogenated and bare diamond (110) surface: a combined LEED-, XPS-, and ARPES study, Surf. Sci. 443 (1999) 177–185. https://doi.org/10.1016/S0039-6028(99)01010-9.

[62] A.K. Tiwari, J.P. Goss, P.R. Briddon, N.G. Wright, A.B. Horsfall, R. Jones, H. Pinto, M.J. Rayson, Calculated electron affinity and stability of halogen-terminated diamond, Phys. Rev. B. 84 (2011) 245305. https://doi.org/10.1103/PhysRevB.84.245305.

[63] G. Kern, J. Hafner, Ab initio calculations of the atomic and electronic structure of clean and hydrogenated diamond (110) surfaces, Phys. Rev. B. 56 (1997) 4203. https://doi.org/10.1103/PhysRevB.56.4203.

[64] A. Gali, E. Janzén, P. Deák, G. Kresse, E. Kaxiras, Theory of spin-conserving excitation of the N− V− center in diamond, Phys. Rev. Lett. 103 (2009) 186404.

https://doi.org/10.1103/PhysRevLett.103.186404.

[65] R.S. Mulliken, The Rydberg States of Molecules.1a Parts I-V1b, J. Am. Chem. Soc. 86 (1964) 3183–3197. https://doi.org/10.1021/ja01070a001.

[66] S. Hadenfeldt, C. Benndorf, Adsorption of fluorine and chlorine on the diamond (100) surface, Surf. Sci. 402–404 (1998) 227–231. https://doi.org/10.1016/S0039-6028(98)00003-X.

[67] K.J. Rietwyk, S.L. Wong, L. Cao, K.M. O'Donnell, L. Ley, A.T.S. Wee, C.I. Pakes, Work function and electron affinity of the fluorine-terminated (100) diamond surface, Appl. Phys. Lett. 102 (2013) 91604. https://doi.org/10.1063/1.4793999.

[68] S. Cui, E.L. Hu, Increased negatively charged nitrogen-vacancy centers in fluorinated diamond, Appl. Phys. Lett. 103 (2013) 51603. https://doi.org/10.1063/1.4817651.

[69] T. Kondo, H. Ito, K. Kusakabe, K. Ohkawa, K. Honda, Y. Einaga, A. Fujishima, T. Kawai, Characterization and electrochemical properties of CF4 plasma-treated boron-doped diamond surfaces, Diam. Relat. Mater. 17 (2008) 48–54. https://doi.org/10.1016/j.diamond.2007.10.009.

[70] R. Löfgren, R. Pawar, S. Öberg, J.A. Larsson, Charged dopants in neutral supercells through substitutional donor (acceptor): nitrogen donor charging of the nitrogen-vacancy center in diamond, New J. Phys. 20 (2018) 23002. https://doi.org/10.1088/1367-2630/aaa382.

[71] R. Löfgren, R. Pawar, S. Öberg, J.A. Larsson, The bulk conversion depth of the NV-center in diamond: computing a charged defect in a neutral slab, New J. Phys. 21 (2019) 53037. https://doi.org/10.1088/1367-2630/ab1ec5.

[72] H.-P. Komsa, T.T. Rantala, A. Pasquarello, Finite-size supercell correction schemes for charged defect calculations, Phys. Rev. B. 86 (2012) 45112. https://doi.org/10.1103/PhysRevB.86.045112.

[73] M.C. da Silva, M. Lorke, B. Aradi, M.F. Tabriz, T. Frauenheim, A. Rubio, D. Rocca, P. Deák, Self-consistent potential correction for charged periodic systems, Phys. Rev. Lett.

126 (2021) 76401. https://doi.org/10.1103/PhysRevLett.126.076401.

[74] G. Davies, M.F. Hamer, W.C. Price, Optical studies of the 1.945 eV vibronic band in diamond, Proc. R. Soc. London. A. Math. Phys. Sci. 348 (1976) 285–298. https://doi.org/10.1098/rspa.1976.0039.

[75] S. Lu, D. Fan, C. Chen, Y. Mei, Y. Ma, X. Hu, Ground-state structure of oxidized diamond (100) surface: An electronically nearly surface-free reconstruction, Carbon N. Y. 159 (2020) 9–15. https://doi.org/10.1016/j.carbon.2019.12.003.

[76] H. Yamano, S. Kawai, K. Kato, T. Kageura, M. Inaba, T. Okada, I. Higashimata, M. Haruyama, T. Tanii, K. Yamada, S. Onoda, W. Kada, O. Hanaizumi, T. Teraji, J. Isoya, H. Kawarada, Charge state stabilization of shallow nitrogen vacancy centers in diamond by oxygen surface modification, Jpn. J. Appl. Phys. 56 (2017) 04CK08. https://doi.org/10.7567/JJAP.56.04CK08.

[77] I. Lovchinsky, A.O. Sushkov, E. Urbach, N.P. de Leon, S. Choi, K. De Greve, R. Evans, R. Gertner, E. Bersin, C. Müller, Nuclear magnetic resonance detection and spectroscopy of single proteins using quantum logic, Science. 351 (2016) 836–841. https://doi.org/10.1126/science.aad8022.

[78] G. Kucsko, P.C. Maurer, N.Y. Yao, M. Kubo, H.J. Noh, P.K. Lo, H. Park, M.D. Lukin, Nanometre-scale thermometry in a living cell, Nature. 500 (2013) 54–58. https://doi.org/10.1038/nature12373.

[79] R. Schirhagl, K. Chang, M. Loretz, C.L. Degen, Nitrogen-vacancy centers in diamond: nanoscale sensors for physics and biology, Annu. Rev. Phys. Chem. 65 (2014) 83–105. https://doi.org/10.1146/annurev-physchem-040513-103659.

[80] S. Li, J.P. Chou, J. Wei, M. Sun, A. Hu, A. Gali, Oxygenated (113) diamond surface for nitrogen-vacancy quantum sensors with preferential alignment and long coherence time from first principles, Carbon N. Y. 145 (2019) 273–280. https://doi.org/10.1016/j.carbon.2019.01.016.

[81] A.M. Edmonds, U.F.S. D'Haenens-Johansson, R.J. Cruddace, M.E. Newton, K.-M. Fu, C.

Santori, R.G. Beausoleil, D.J. Twitchen, M.L. Markham, Production of oriented nitrogen-vacancy color centers in synthetic diamond, Phys. Rev. B. 86 (2012) 35201. https://doi.org/10.1103/PhysRevB.86.035201.